physica status solidi a
www.pss-a.com
applications and materials science

Identification and carrier dynamics of the dominant lifetime limiting defect in n⁻ 4H-SiC epitaxial layers

Feature Article

P. B. Klein[*]

Naval Research Laboratory, 4555 Overlook Avenue SW, Washington DC 20375, USA

[*] e-mail klein@bloch.nrl.navy.mil

The identity and characteristics of the lifetime limiting defects in n-type 4H-SiC epitaxial layers are of particular current interest, due to the suitability of this material for high-power, solid-state switching devices. Much work has been done in the past decade to identify the spectral signature and the local atomic structure of the defect that controls the lifetime in this material. Until recently, it was concluded that two dominant electron traps, $Z_{1/2}$ and $EH_{6/7}$, both associated with a carbon vacancy, were controlling the lifetime. DLTS and optical studies show, however, that $EH_{6/7}$ is not an important minority carrier trap, due to its small capture cross section for holes. Thus, $Z_{1/2}$ acts alone as the lifetime limiting defect. The details of recombination at this trap have been studied through the injection level and temperature dependence of the carrier lifetime and through carrier dynamics simulations that take into account the complex nature of the defect. The simulations shed light on the processes that dominate the recombination at $Z_{1/2}$ over a large range of injection level and temperature.

1 Introduction Wide bandgap semiconductors are of great current interest, as their material properties – high thermal conductivity, high breakdown voltage, high thermal stability and chemical inertness – make them ideal for applications that demand high power and/or high frequency operation that is well beyond the limitations of Si-based technology. Consequently, there is much interest in these systems for high power solid-state switching and communications applications. As a result, much research has been carried out in the direct-gap GaN and GaN/AlGaN systems for high power, high frequency microwave transistors and in SiC (indirect band gap) for high power bipolar switching devices.

SiC grows in numerous possible stacking orders (polytypes), each with a distinct bandgap. The most common polytypes are 3C (cubic, zincblende structure, $E_g = 2.36$ eV), 6H and 4H (hexagonal, wurtzite structure, $E_g = 3.0$ eV and 3.23 eV, respectively). For applications involving high-voltage bipolar switching devices, it is clear from a comparison of typical material parameters for GaN and SiC to those of Si, shown in Table 1, that the combination of high thermal conductivity and high breakdown field provides SiC with a distinct advantage over both GaN and Si. The 4H polytype of SiC is favored over 6H in these high power vertical devices because of its much higher mobility along the c-axis, which is the growth direction in most epitaxial layers.

High power switching devices, such as p–i–n diodes and insulated-gate bipolar transistors, require a thick, low-doped drift layer to provide the low conductivity necessary to hold off a high voltage across the device when the switch is in the off-state. This is facilitated by the high breakdown field of SiC. With the switch in the on-state, however, the same n⁻ drift region must have a *high* conductivity, in order to assure a low forward voltage drop and low power dissipation. This duality in the conductivity of the drift layer is made possible by the process of conductivity modulation, whereby a high concentration of minority carriers (and majority carriers) are injected into the drift region under high forward bias, resulting in a large en-

Report Documentation Page

Form Approved OMB No. 0704-0188

Public reporting burden for the collection of information is estimated to average 1 hour per response, including the time for reviewing instructions, searching existing data sources, gathering and maintaining the data needed, and completing and reviewing the collection of information. Send comments regarding this burden estimate or any other aspect of this collection of information, including suggestions for reducing this burden, to Washington Headquarters Services, Directorate for Information Operations and Reports, 1215 Jefferson Davis Highway, Suite 1204, Arlington VA 22202-4302. Respondents should be aware that notwithstanding any other provision of law, no person shall be subject to a penalty for failing to comply with a collection of information if it does not display a currently valid OMB control number.

1. REPORT DATE **FEB 2009**	2. REPORT TYPE	3. DATES COVERED **00-00-2009 to 00-00-2009**
4. TITLE AND SUBTITLE **Identification and carrier dynamics of the dominant lifetime limiting defect in n- 4H-SiC epitaxial layers**		5a. CONTRACT NUMBER
		5b. GRANT NUMBER
		5c. PROGRAM ELEMENT NUMBER
6. AUTHOR(S)		5d. PROJECT NUMBER
		5e. TASK NUMBER
		5f. WORK UNIT NUMBER
7. PERFORMING ORGANIZATION NAME(S) AND ADDRESS(ES) **Naval Research Laboratory,4555 Overlook Avenue SW,Washington,DC,20375**		8. PERFORMING ORGANIZATION REPORT NUMBER
9. SPONSORING/MONITORING AGENCY NAME(S) AND ADDRESS(ES)		10. SPONSOR/MONITOR'S ACRONYM(S)
		11. SPONSOR/MONITOR'S REPORT NUMBER(S)

12. DISTRIBUTION/AVAILABILITY STATEMENT **Approved for public release; distribution unlimited**

13. SUPPLEMENTARY NOTES

14. ABSTRACT

15. SUBJECT TERMS

16. SECURITY CLASSIFICATION OF:			17. LIMITATION OF ABSTRACT	18. NUMBER OF PAGES	19a. NAME OF RESPONSIBLE PERSON
a. REPORT **unclassified**	b. ABSTRACT **unclassified**	c. THIS PAGE **unclassified**	**Same as Report (SAR)**	**16**	

Standard Form 298 (Rev. 8-98)
Prescribed by ANSI Std Z39-18

Table 1 Comparison of material properties of Si, SiC and GaN.

	E_g (eV)	μ_n (cm²/V s)	E_{BRK} (MV/cm)	λ (W/cm K)
Si	1.1	1350	0.3	1.5
3C-SiC	2.36	900	1.2	4.5
4H-SiC	3.23	720 ∥ a 650 ∥ c	2.0	4.5
6H-SiC	3.20	370 ∥ a 50 ∥ c	2.4	4.5
GaN	3.39	900	3.3	1.3

hancement in the conductivity of the layer. The degree to which conductivity modulation is effective in providing the necessary high carrier concentration to the drift layer is directly related to the lifetime of the minority carriers within the region: a short carrier lifetime results in limited conductivity modulation and a large forward voltage drop. Consequently, understanding the limitations on the carrier lifetime has become a topic of intense interest. The carrier lifetime in the drift region affects not only the conductivity of the layer under forward bias, but also the switching speed of the device: Longer lifetimes afford better conductivity modulation but also slower switching speeds. Consequently, device design requires a compromise between these two parameters, so it is necessary to be able to tailor the carrier lifetime for a particular device. This kind of lifetime control can be achieved if the minority carrier lifetime in the as-grown drift layer can be made longer than required and if a post-growth process, such as electron irradiation, is developed to reduce the lifetime in a controlled manner to the required level [1]. Both conductivity modulation and lifetime control require long carrier lifetimes.

The primary mechanism responsible for reducing the carrier lifetime is the trapping of free carriers at material defects. Consequently, it has become important to identify and to characterize the specific defects that dominate the trapping of minority carriers and thus control the carrier lifetime within the drift region. In Section 2 we review briefly the evolution, over the last 10–15 years, of a) the microscopic structures that have been associated with the dominant defects, and b) the correlation between the carrier lifetime and specific defects. The progress toward identifying the responsible recombination centers led to the conclusion that the lifetime limiting defects were the two dominant electron traps observed in deep level transient spectroscopy (DLTS) measurements of as-grown epilayers, labeled as $Z_{1/2}$ (or Z1/Z2) and $EH_{6/7}$ (or EH6/EH7). However, evidence presented in Section 3 indicates that it is only $Z_{1/2}$ that has a significant effect upon the carrier lifetime. The processes controlling the carrier dynamics at this defect are considered in detail in Section 4, both through experiment and through carrier dynamics simulations, in order to provide a deeper understanding of recombination at this defect and of those parameters that significantly affect the lifetime. The discussion is summarized in Section 5.
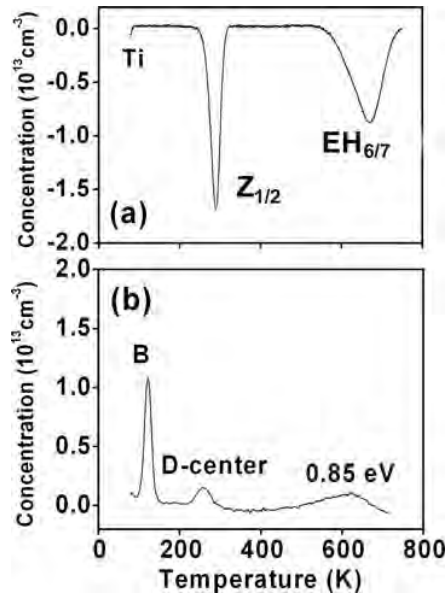
Figure 1 DLTS (a) and MCTS (b) spectra of typical n-type 4H-SiC epitaxial layers. (Adapted from Ref. [2].)

The DLTS spectrum of a typical as-grown, n-type epitaxial layer of 4H-SiC, similar to that shown in Fig. 1(a) [2], is dominated by the two electron traps, generally referred to as $Z_{1/2}$ ($\approx E_c - 0.65$ eV) and $EH_{6/7}$ ($\approx E_c - 1.65$ eV). Each of these designations refers to two similar but distinguishable defects, Z_1, Z_2 and EH_6, EH_7 – each pair thought to be the same defect on cubic and hexagonal lattice sites [3]. Other traps are often observed, such as Ti ($E_c - 0.17$ eV), but usually at lower concentrations. Minority carrier transient spectroscopy (MCTS) measurements in as-grown material, similar to that shown in Fig. 1(b) [2], are generally dominated by two persistent boron-related hole traps: the shallow boron acceptor ($E_v + 0.27$ eV) and the D-center ($E_v + 0.65$ eV), a boron-related complex [4, 5]. DLTS, in conjunction with carrier lifetime measurements, has been central in the effort to identify the defects that control the carrier lifetime. Much of this work has been focused on either a) identifying the atomic structure of important traps, by correlating DLTS features with varying growth or post-growth processing conditions, or b) identifying the traps that limit the carrier lifetime, through correlations between DLTS measurements and carrier lifetime measurements. Initially, these two approaches were taken almost independently, with significant overlap occurring only later. Consequently, the discussion of this work will treat each approach separately, beginning with the former.

2 Defects in 4H-SiC epilayers
2.1 Defect structure The application of DLTS measurements to the study of deep traps in 4H-SiC was first carried out on bulk n-type samples grown by sublimation vapor transport by Uddin et al. [6]. The spectra were dominated by a broad peak due to an electron trap near

Phys. Status Solidi A **206**, No. 10 (2009)

2259

$E_c - 0.72$ eV, which was thought to be associated with a defect at both cubic and hexagonal sites. DLTS measurements on epitaxial layers of n-type 4H-SiC were initially investigated by Kimoto et al. [7], who observed a similar, dominant electron trap, $\approx 0.61 - 0.68$ eV below the conduction band. This defect was noted to be similar to the Z_1/Z_2 center reported in 6H-SiC by Pensl and Choyke [8] and by Zhang [9, 10]. This designation was adopted in 4H-SiC as well. Doyle et al. [11] reported a similar dominant trap in as-grown 4H-SiC that evolved into two closely-spaced levels after electron irradiation. A similar broadening of the Z_1 DLTS spectrum after He$^+$ ion implantation, due to the generation of a second, similar defect, was observed by Dalibor et al. [12, 13], who found that the Z_1 component behaved as an acceptor and was found to be thermally stable above 2000 °C, while the second component annealed out near 1000 °C. This was interpreted as evidence that the latter component was a single intrinsic defect. Using the previously published association of the Z-center with the D1 photoluminescence (PL) band [14] in 6H-SiC, the authors concluded from low temperature PL and DLTS studies that the $Z_{1/2}$ center was consistent with a nearest-neighbor $V_C - V_{Si}$ divacancy. However, the D1-$Z_{1/2}$ association in 4H-SiC was later shown to be erroneous [15]. The EH$_{6/7}$ defect was introduced by Hemmingsson et al. [16], appearing as a broad peak (reflecting two defects, EH$_6$ and EH$_7$) in the DLTS spectra of as-grown and electron-irradiated samples, with an acceptor level at $E_c - 1.65$ eV and a large electron capture cross-section ($\sigma_n > 5 \times 10^{-15}$ cm^2).

The broad DLTS signature for $Z_{1/2}$ was shown by Hemmingsson et al. [3, 17] to result from the fact that the defect is a negative-U center and thus able to trap two electrons. This results in three possible charge states (empty, singly- and doubly-occupied). Consequently, there are two transitions within the gap; a (0/+) donor state and a (–/0) acceptor state that lies deeper in the band gap, due to large lattice relaxation around the negatively charged center. As a result, during a standard DLTS temperature scan thermal ionization of an electron from the doubly-occupied "–" state led to the immediate ionization of the resulting, shallower "0" state, so that an effective –/+ transition was observed. Hence, only the single, broad $Z_{1/2}$ signature reflecting the –/+ transition was seen in DLTS, as shown [3] in Fig. 2(a). The signature of the "0" state was not observed. By initially emptying the "–" state with a light pulse and using very short filling pulse widths to minimize any initial capture of carriers back into the "–" state, the DLTS signature of the 0/+ transition for both Z_1 and Z_2 were revealed, as shown in Fig. 2(b). The configuration coordinate diagram of the three $Z_{1/2}$ charge states in the inset reflected the large lattice relaxation of the "–" state.

While several defects were reported from DLTS studies, there was little progress in identifying the chemical nature of these traps until systematic studies were carried out to determine the effect of varying growth conditions and post-growth processing on defect concentrations. In the case of $Z_{1/2}$, this led to a long series of contradictory identi-
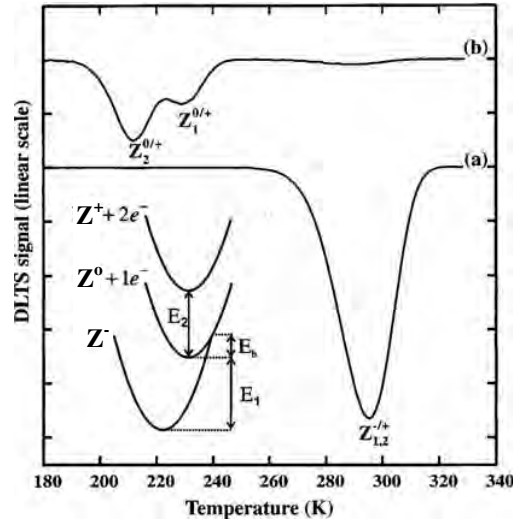
Figure 2 DLTS specta (a) of the $Z_{1/2}$ (–/+) transition, and (b) of the $Z_{1/2}$ (0/+) transition, obtained by pre-irradiating the sample and using short filling pulses. The configuration coordinate diagram in the inset reflects the negative-U property of the defect. (Adapted from Ref. [3].)

fications. By investigating the effect of a varying C/Si ratio on the formation of Z_1 defects during CVD growth, Kimoto et al. [18] observed a decrease in the defect concentration for C-rich growth conditions, concluding that Z_1 was an intrinsic defect, most probably a Si antisite (Si$_C$) or C vacancy (V_C). On the other hand, Kawasuso et al. [19] compared the concentrations of $Z_{1/2}$ defects, measured by DLTS, and vacancies, detected by positron annihilation studies, as a function of thermal annealing temperature. The similarity in their annealing behavior led to the conclusion that the defect was related to Si vacancies (V_{Si}). Another alternative origin for the $Z_{1/2}$ center was suggested from the work of Pintilie et al. [20], where the defect concentration was positively correlated with the nitrogen doping level and the C/Si ratio. However, the $Z_{1/2}$ concentration was observed to increase with more C-rich growth conditions, which is opposite to previous [18] and later reports. As a result of these investigations, the $Z_{1/2}$ center was assigned to a substitutional N – interstitial C complex, N-C$_i$. This view was supported by theoretical calculations [21] suggesting that the $Z_{1/2}$ center was consistent with an interstitial N – interstitial C complex, N$_i$–C$_i$. However, the involvement of N in the composition of the $Z_{1/2}$ defect was later refuted [22–24].

A detailed study of the effect of varying growth conditions (growth temperature, C/Si ratio and sample position relative to the gas flow) on the incorporation of defects was carried out by Zhang et al. [25] for the Ti and B impurities, the HS1 hole trap and the $Z_{1/2}$ and EH$_{6/7}$ electron traps. The latter two defects exhibited a very similar dependence on growth temperature (with a formation energy near 4 eV), similar variations in concentration along the di-
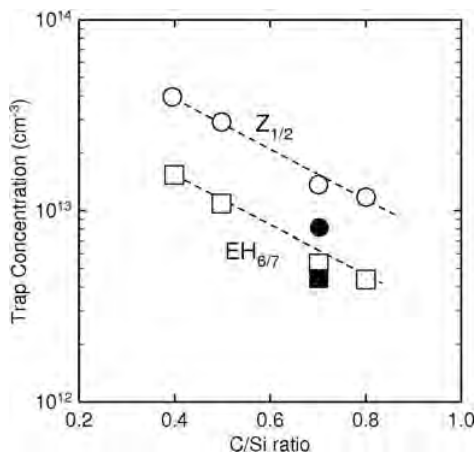
Figure 3 Similar dependences of the $Z_{1/2}$ and $EH_{6/7}$ concentrations on C/Si ratio. (Adapted from Ref. [27].)

rection of gas flow and a relatively weak dependence on C/Si ratio over the range that was studied. From these results it was concluded that the $Z_{1/2}$ center was consistent with a divacancy, an antisite pair or an antisite-vacancy pair, while the $EH_{6/7}$ defect was tentatively associated with the carbon vacancy. Kimoto et al. [26] found a very different dependence on C/Si ratio for $EH_{6/7}$ and $Z_{1/2}$, which was consistent with their earlier work: The concentrations of *both* defects decreased significantly as the growth became more C-rich. This dependence upon C/Si ratio was later shown [27, 28] to be essentially the same for both defects, as shown [27] in Fig. 3. The two defects were also found [29, 30] to exhibit a very similar dependence upon thermal anneal temperature (Fig. 4) – both were found stable to at least 1600 °C and decreased by an order of magnitude at higher temperatures. All of these similarities suggested that the two defects might both be related to the same center, such as a V_C.

Storasta et al. [23] investigated the defect formation and annealing properties of samples exposed to low energy electron irradiation that was below the threshold for Si
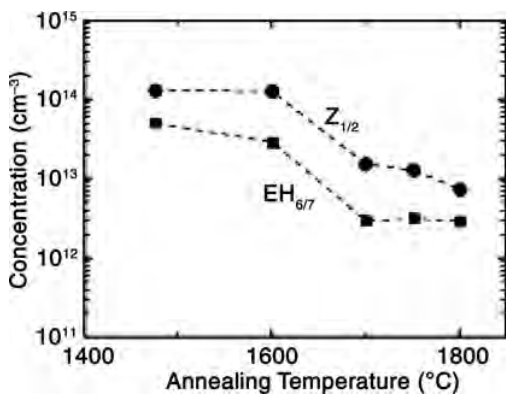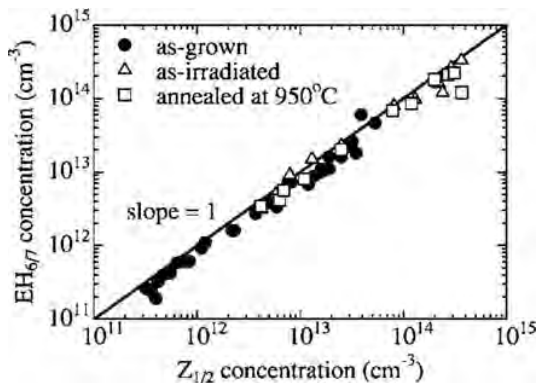
atom displacement. Consequently, only intrinsic defects related to the initial displacement of carbon atoms from their lattice sites were created. The irradiation-induced defects that resulted were $Z_{1/2}$ and $EH_{6/7}$, as well as the EH1 and EH3 electron traps and the HS2 hole trap. Because only carbon atoms were displaced, it was concluded that the appearance of these defects was found consistent with structures involving V_C, C_i C_{Si} and Si_C, while divacancies, diinterstitials and impurity complexes (including N-defect complexes) were ruled out. These results put strict limitations on the microscopic structures that were possible for these defects. Danno et al. [31] suggested that the characteristics of the $EH_{6/7}$ defect were consistent with the acceptor state of the V_C, and that the isolated V_C may be associated with the P1 hole trap in p-type material. A further study by Litton et al. [32] of the effect of C/Si ratio on $Z_{1/2}$ concentration concluded that the defect was either V_C or Si_C-related.

Overall, the evidence described above, developed over a substantial period of time, indicated that both $Z_{1/2}$ and $EH_{6/7}$ appear to behave similarly with varying growth conditions (C/Si ratio, growth temperature) or post-growth processing (thermal anneal, electron irradiation), suggesting that both centers may be related to the same intrinsic defect. This picture has been confirmed recently [33], verifying many of these observations within the same group of samples and showing (Fig. 5) that, for a large number of as-grown, electron-irradiated and irradiated/annealed samples, there is a one-to-one correlation between the concentrations of $Z_{1/2}$ and $EH_{6/7}$. As both defects have also been shown to be consistent with the involvement of a carbon vacancy, the current view is that both of these defects are V_C-related centers.

It was also noted [33] that while the energy levels within the band gap for these two defects were shown to be consistent with the energy level positions of different charge states of the isolated V_C, determined from theoretical calculations [34, 35] and by photo-EPR measurements [36], the involvement of a V_C-related complex could not be

Figure 4 Similar dependences of the $Z_{1/2}$ and $EH_{6/7}$ concentrations on anneal temperature. (Adapted from Ref. [29].)

Figure 5 Correlation between $Z_{1/2}$ and $EH_{6/7}$ concentrations for a large range of 4H-SiC epilayers. Reprinted with permission from Ref. [33], © 2006, American Institute of Physics.

Phys. Status Solidi A **206**, No. 10 (2009)

2261

ruled out. The picture becomes somewhat more complex when the correlation between calculated defect properties and experimental results includes, in addition to energy levels, the donor or acceptor nature of the defect states and whether the defect forms a –U center. With these considerations in mind, Eberlein et al. [37] concluded that while both $Z_{1/2}$ and $EH_{6/7}$ could be consistent with different V_C charge states, other possibilities exist, such as the assignment of $Z_{1/2}$ as a C_i-complex. Thus far, a definitive identification of the detailed local structure of these defects has yet to be made.

2.2 Carrier lifetime studies Initial investigations of the minority carrier lifetime (MCL) in 4H-SiC epitaxial materials were primarily carried out using optical techniques; time-resolved photoluminescence (TRPL) of the near-band edge emission at room-temperature, transient free carrier absorption (TFCA) and microwave photoconductivity decay (μ-PCD). Using low-injection TRPL, Kordina et al. [38] found that the MCL exhibited a significant spatial variation across the wafer, with lifetime mapping indicating variations from <0.5 μs to 2.1 μs, suggesting good material quality on portions of the wafer. These variations in lifetime were found correlated with the morphology of the wafer, suggesting that structural defects could affect the lifetime. Galeckas et al. [39] used TFCA to observe similar values for the carrier lifetime, albeit under higher excitation conditions. Evidence of contributions to the lifetime from surface and Auger recombination was also investigated. Spatial scanning provided TFCA lifetime maps that also reflected a correlation of structural defects with the lifetime. Using depth profiling, TFCA measurements [40] also provided the time-dependent depth distribution of the injected carrier concentration, thus enabling the determination of surface recombination velocities associated with the surface and with the n^-/n^+-substrate interface. This demonstrated the extent to which the surface could play an important role in limiting the carrier lifetime, particularly in thinner layers.

While the present focus is on point defects that limit the carrier lifetime, the observation of lifetime correlations with structural defects serves as a reminder that under the right conditions, other processes can also make significant contributions. TRPL mapping has shown, for example, that the lifetime can be influenced by structural defects in the substrate that propagate into the epilayers, and that correlation of the lifetime maps with X-ray topography studies associates reduced carrier lifetimes with small angle grain boundaries containing threading edge dislocations [41, 42]. However, while the observation that structural defects can affect the lifetime is well documented, their precise role is still unclear. For example, it has been reported [43] that the carrier lifetime in bulk wafers *increases* near regions of high defect density, due to the gettering of point defects by the structural defects. Similarly, the Z_1 concentration has been observed to decrease in epitaxial layers containing higher dislocation densities [44]. Structural defects that in-

volve local regions of a lower band gap SiC polytype, such as 3C inclusions in 4H, can also trap carriers. Stacking faults (SF's), for example, made up of a few atomic layers of 3C within the 4H epilayers, effectively act as quantum wells [45] that can efficiently trap carriers and reduce the carrier lifetime in the region near the SF [46]. As structural defects are localized, their influence on the bulk lifetime will depend in part on the fraction of the epilayer volume that they influence. Consequently, when there are high concentrations of structural defects, they can be effective in trapping carriers and can contribute significantly to limiting the measured lifetime.

The first real attempt to combine DLTS with carrier lifetime measurements, in order to identify the point defects controlling the lifetime in 4H-SiC, was reported by Storasta et al. [47], who found a direct correlation between an increasing concentration of shallow boron centers and the decrease in the carrier lifetime measured by TRPL. Although this result has not been reproduced in the literature, the authors were careful to point out several specific difficulties with simply assigning boron as the lifetime killer based on these measurements. This also illustrates the fact that, while correlation is a highly valuable tool that aids in associating specific defects with observed material properties, interpretations based on correlations alone must be made with caution.

In addition to correlating DLTS signatures with growth and processing conditions, as described above, Zhang et al. [25] also found that variations in defect concentrations across the wafer were directly correlated with the carrier lifetime determined by TRPL. The results, shown in Fig. 6,
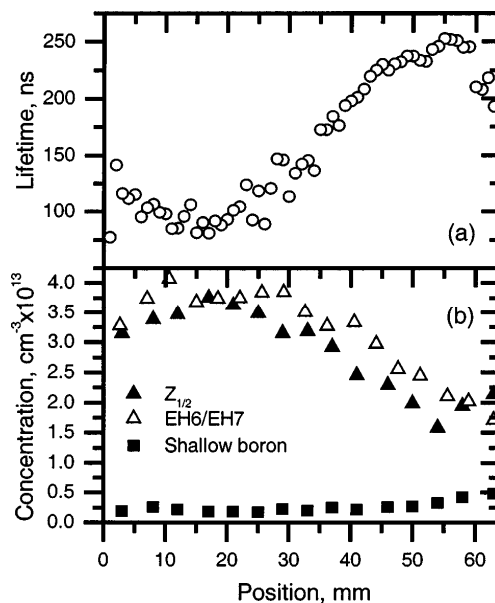
Figure 6 Correlation between $Z_{1/2}$ and $EH_{6/7}$ concentrations and the carrier lifetime, for different sample positions along the gas flow direction. Reprinted with permission from Ref. [25], © 2003, American Institute of Physics.

indicated no obvious relationship between the carrier life-time and the concentration of shallow B, but did indicate a clear relationship between the decrease in the lifetime and the increase in the concentrations of both $Z_{1/2}$ and $EH_{6/7}$. This result led to the conclusion that *both* defects were responsible for limiting the carrier lifetime. A similar correlation (measured by μ-PCD and TRPL) between the lifetime and both the $Z_{1/2}$ and $EH_{6/7}$ concentrations was obtained by Tsuchida et al. [48], who also noted a lack of correlation between the carrier lifetime and the D_1-center or with the concentrations of several impurities. This behavior was also consistent with the later observations of Jenny et al. [49], who demonstrated that the high-temperature annealing of bulk, high purity 4H-SiC substrates to 2600 °C resulted in a dramatic increase in the carrier lifetime (<10 μs to >3 μs) as well as a dramatic decrease in both the $Z_{1/2}$ and $EH_{6/7}$ defect concentrations. The above observations were all taken as evidence that both defects were controlling the carrier lifetime in the n-type epilayers. While this conclusion is quite reasonable given the experimental evidence, it is not the only possible interpretation.

We have already seen that the concentrations of these two defects generally vary in the same way with changes in various growth or post-growth processing conditions, such as varying C/Si ratio, growth temperature, irradiation/implantation and annealing (see e.g. Figs. 3–6). This has been interpreted as reflecting the fact that both centers share the same intrinsic defect in their structure, most probably a V_C. It follows then, that no matter what parameter is varied to effect a change in the defect concentration (and thus in the carrier lifetime), the concentrations of these two defects will usually both respond in a similar way to this changing parameter. Even if only one of the two defects actually has any effect on the carrier lifetime, a correlation of lifetime vs. defect concentration will show a similar variation for *both* defects, simply because both defect concentrations always vary similarly in response to a changing growth or processing parameter. In effect – the lifetime is varying in response to a change in the concentration of one defect, the lifetime-killing defect, while the concentration of the second defect is simply varying with environment in the same way as the first defect, and has no effect on the lifetime. Consequently, it appears that both defects are correlated with the lifetime, when in fact only one is actually responsible for the reduction observed in the carrier lifetime.

In Section 3.2 it is shown that this is, in fact, the case for 4H-SiC: $EH_{6/7}$ does not significantly affect the carrier lifetime, while $Z_{1/2}$ is identified as the dominant lifetime killer. While both of these defects have large electron capture cross-sections and both are deep levels, it is shown that what distinguishes the two defects is that $EH_{6/7}$ has a small capture cross-section for minority holes. Consequently, $Z_{1/2}$ is an effective recombination center and minority carrier trap while $EH_{6/7}$ is limited to the role of an effective majority carrier trap.

3 Identification of the lifetime killer

3.1 Experimental Samples were grown by silane-based MOCVD on n⁺ 4H-SiC substrates, with carrier concentrations ≈mid-10^{14} cm⁻³ and thicknesses ranging from 9–104 μm [2]. DLTS spectra were obtained in the usual way [2], while MCTS measurements employed optically injected pulses from a 365 nm, light emitting diode instead of electrical injection. DLTS spectra were also measured on similarly grown 1.2 mm diameter p–i–n diodes with n-layer thicknesses of 30–100 μm. Time-resolved photoluminescence measurements were carried out at 300 K and excited with either a frequency-tripled, Q-switched Nd:YAG laser (355 nm) or a frequency doubled, cavity-dumped, modelocked Ti:sapphire laser (355 nm, <0.1–1 MHz). The collected light was dispersed by a 0.22 m. double spectrometer and detected by a GaAs photomultiplier and time correlated single photon counting.

3.2 $Z_{1/2}$ or $EH_{6/7}$? In order to investigate the properties of these two defects, DLTS measurements were employed to determine defect concentrations, while low-injection TRPL provided a measure of the minority carrier lifetime. The defect concentrations are expected to be directly related to the bulk MCL due to trapping at defects:

$$\tau_{bulk}^{-1} = \sigma_p v_{th} N_T , \qquad (1)$$

where σ_p is the minority carrier (hole) capture cross-section, v_{th} the carrier thermal velocity, $v_{th} = (3\, kT/m^*)^{1/2}$, and N_T the defect concentration. Carrier lifetime measurements, however, determine only an effective lifetime, τ_{eff}, which generally reflects contributions from capture and emission at defects, i.e. Shockley–Read–Hall recombination (SRH) [50, 51], as well as from other competing recombination processes, such as Auger recombination, surface recombination and radiative recombination:
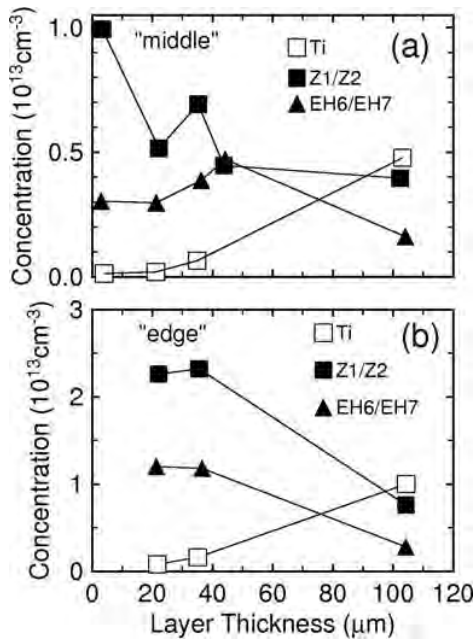
$$\frac{1}{\tau_{eff}} = \frac{1}{\tau_{bulk}(SRH)} + \frac{1}{\tau_{Rad}} + \frac{1}{\tau_{Auger}} + \frac{1}{\tau_{Surf}} . \qquad (2)$$

Because SiC is an indirect band gap material, the recombination of free electrons with free holes is a very slow process. Consequently, the carrier lifetime is determined by the much faster competing processes. Hence, phonon-assisted radiative processes contribute only a small fraction to the total recombination rate. For low-to-moderate injection conditions, Auger recombination is negligible. Thus, the bulk lifetime is dominated by SRH recombination. Surface recombination, however, cannot be ignored, particularly for thin epitaxial layers. Consequently, in order to relate the bulk lifetime with the concentration of a particular defect using Eq. (1), the bulk lifetime must be extracted from the measured *effective* lifetime. This requires determining the surface recombination rate, $(\tau_{Surf})^{-1}$, which can be reasonably approximated by [52]

$$\frac{1}{\tau_{Surf}} = \left(\frac{d^2}{\pi^2 D} + \frac{d}{2S} \right)^{-1} , \qquad (3)$$

where d is the layer thickness, D the injection-dependent diffusion coefficient for 4H-SiC [53], and S represents an average surface recombination velocity for the layer. Consequently, one way to extract the bulk and surface lifetimes for a group of similar samples (i.e. assuming similar surface recombination) is to measure the dependence of the lifetime on layer thickness, d. A set of epitaxial layers was grown [2] for this purpose with a range of layer thicknesses varying from 9 μm to 104 μm.
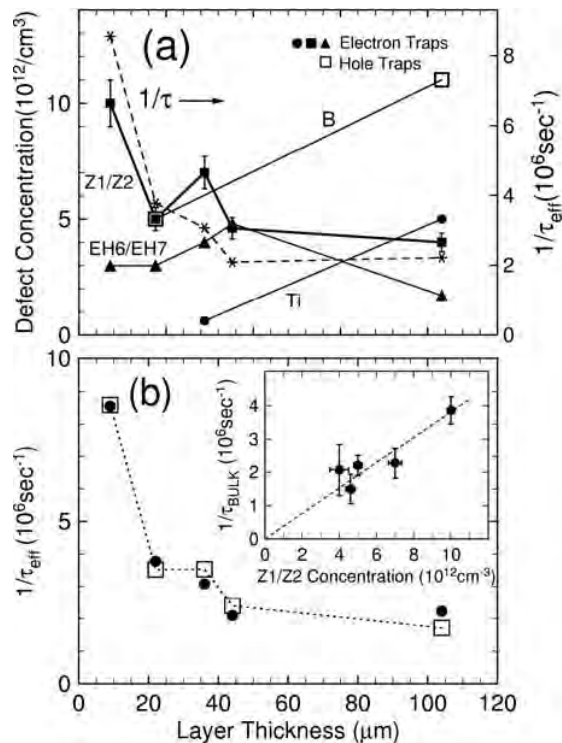
DLTS and lifetime measurements were carried out on material taken from the center, middle and edge of each wafer. The variation in the concentrations of $Z_{1/2}$, $EH_{6/7}$ and Ti centers are shown as a function of layer thickness for "middle" and "edge" samples in Fig. 7(a) and (b), respectively [54, 55]. For the latter, the $Z_{1/2}$ and $EH_{6/7}$ concentrations show similar behavior, in agreement with the numerous reports discussed above. For the "middle" samples, however, there is a clear difference in the variations of the concentrations of these two defects with layer thickness. It can be noted that there is a general trend toward lower intrinsic defect concentrations for thicker layers. While the cause of this is unclear, Fujihira et al. [56] have speculated that the stress between the epilayer and substrate leads to a higher defect concentration, and that trap formation may consequently be reduced in the thicker layers. It should also be noted that these variations in the defect concentrations for different thickness wafers do not conflict with the observed lack of any significant variation in defect concentration across the thickness of a single layer, recently reported by ul Hassan et al. [57]. In any case, the different

dependences of the concentrations of these two defects on varying layer thickness, as in Fig. 7(a), provides an opportunity to make a meaningful comparison between their measured defect concentrations and the carrier lifetime. The variation in concentration of $Z_{1/2}$, $EH_{6/7}$, shallow B and Ti centers are shown in Fig. 8(a) and are compared to the inverse of the effective carrier lifetime, as measured by low-injection TRPL. It is apparent from the figure that only the $Z_{1/2}$ concentration exhibits any clear correlation with $1/\tau_{eff}$. This is, perhaps, a first indication that only one of these defects may limit the lifetime.

The measured dependence of the inverse effective lifetime on layer thickness may be fitted using Eqs. (1)−(3), with only SRH (bulk) and surface contributions. The result of this fit is shown as the open squares and dotted line in Fig. 8(b) and compared to the measured values (solid circles). The fitted curve is not smooth because *measured* defect concentrations were used rather than requiring an additional fitting parameter. The best fit parameters were found to be $S = 1250$ cm/s and $\sigma_p = 3.5 \times 10^{-14}$ cm^2 [2]. From this, *bulk* lifetimes could be extracted, and are plotted as a function of $Z_{1/2}$ concentration in the inset of the figure. The linear relationship again suggests that $Z_{1/2}$ is the responsible defect.

Figure 7 Variation of defect concentrations with layer thickness for samples obtained from the "middle" (a) and "edge" (b) regions of each wafer. (Adapted from Ref. [54].)

Figure 8 (a) Variation of defect concentrations and the inverse of the TRPL decay time on layer thickness, and (b) fit (open squares) of the lifetime data (filled circles) using Eqs. (1)−(3). The inset plots the extracted bulk lifetimes vs. $Z_{1/2}$ concentration. Reprinted with permission from Ref. [2], © 2006, American Institute of Physics.

Thus far, $EH_{6/7}$ has been ruled out as a lifetime-limiting defect based only on the lack of correlation between the defect concentration and the carrier lifetime within this particular group of "middle" samples. However, a less sample-dependent procedure to test the role of $EH_{6/7}$ in reducing the lifetime is preferable. This was carried out by DLTS measurements in a p–i–n diode structure [2, 54]. Under a large forward bias, the drift region of the diode is flooded with a high concentration of minority holes. The filled electron traps $Z_{1/2}$ and $EH_{6/7}$ would be expected to trap these holes, changing their charge states and consequently reducing the strength of their DLTS signatures. Figure 9(a) shows a plot of DLTS signal strength vs. forward bias for both defects. Above 2 V the standard $Z_{1/2}$ (–/+) signature is totally quenched and a (0/+) signal appears – both resulting from the capture of minority holes by the doubly-occupied $Z_{1/2}$. However, the $EH_{6/7}$ signal is not significantly affected by the large injected hole concentration, indicating that this defect must have a small capture cross-section for minority holes. This observation has recently been confirmed by Reshanov et al. [58], as shown in Fig. 9(b). With a small hole capture cross section, $EH_{6/7}$ cannot be responsible for trapping minority carriers and limiting the MCL. Therefore, $Z_{1/2}$ alone must be the lifetime killer. The carrier dynamics at this defect, which determine the MCL, will be considered in detail in a later section.
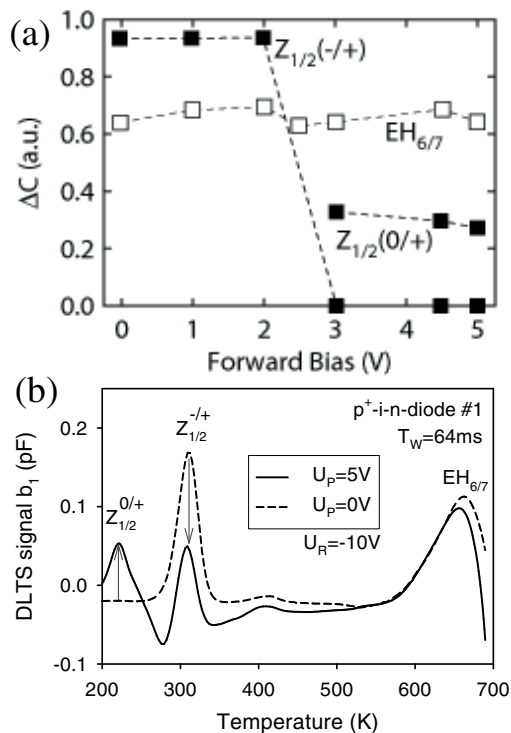
Figure 9 (a) Variation of the DLTS signals for $Z_{1/2}$ and $EH_{6/7}$ defects as a function of forward bias in a p–i–n diode. (Adapted from Ref. [54]). These observations were verified independently in (b) [58], © Trans-Tech Publications, 2009.

3.3 Recent developments Recently, there has been further support of the view that $Z_{1/2}$ and $EH_{6/7}$ are related to the V_C. Danno et al. [28] have determined that the formation of these defects is independent of growth rate, and depends primarily upon C/Si ratio and growth temperature. The dependence upon the latter provided an activation energy that was found consistent with a simple thermodynamic model for the carbon vacancy. The authors also argued that the thermal stability of the defects was consistent with a V_C, but not with C-interstitials. This view was supported by Storasta et al. [59], who demonstrated that C-implantation and annealing led to a dramatic decrease in the $Z_{1/2}$ and $EH_{6/7}$ concentrations and a doubling of the carrier lifetime, which was discussed in terms of the diffusion of implantation-induced C-interstitials and subsequent annihilation of carbon vacancies. It was later shown [60] that this approach resulted in thick epitaxial layers with a $Z_{1/2}$ concentration $<10^{11}$ cm^{-3}, with resulting device structures that exhibited good conductivity modulation. By measuring the dependence of the carrier lifetime over a large range of $Z_{1/2}$ concentrations, Danno et al. [61] have shown that below about 10^{13} cm^{-3} the carrier lifetime becomes sub-linear with $Z_{1/2}$ concentration, and at even lower concentrations it becomes independent of $Z_{1/2}$. At this stage, it is apparent that the contribution by this defect to the inverse lifetime (e.g. Eqs. (1) and (2)) has become small compared to other sources, such as surface recombination or carrier capture by other defects. It should be noted, however, that the concentration (10^{13} cm^{-3}) at which this transition occurs will be sample-dependent, as the surface condition and the concentrations of other defects will clearly vary between different samples. While the defect or surface recombination that controls the lifetime in low-$Z_{1/2}$ material may not compromise the lifetime sufficiently to be a major problem for lower-voltage bipolar devices, in high voltage switches, where the drift layer must be thick and the MCL must be very long, these remaining limits to the carrier lifetime can become problematic.

As $Z_{1/2}$ is the dominant lifetime killer when present in sufficient concentration, it is of interest to examine the processes associated with carrier capture at this defect, in order to gain a better understanding of its unique role and of the important parameters that determine the lifetime. This is considered in detail in the following section.

4 Carrier dynamics at the $Z_{1/2}$ defect
4.1 Introduction A study of the dominant processes controlling carrier capture and emission at the lifetime limiting defect in 4H-SiC epilayers provides an understanding of the key parameters that affect the lifetime, both in as-grown material and in device structures. The wide variation in carrier lifetimes appearing in the literature can be understood to result from differences in the experimental conditions under which the measurements are carried out (e.g. injection level, temperature), differences in material quality (defect concentrations, surface condition), or even in the choice of experimental measurement technique, as

different measurements can be sensitive to qualitatively different lifetimes [62]. Consequently, minority carrier lifetime measurements carried out at low injection in as-grown material can be very different from the lifetime in a device that has been subsequently fabricated from the same material and operating under high injection conditions and at elevated temperature. For carrier dynamics determined by SRH recombination at a given temperature, the lifetime of the minority carriers increases with injection level from the low-injection limit (τ_{MCL}) dominated by minority carrier capture, to the high injection limit (τ_{HL}), where non-equilibrium electron and hole concentrations and lifetimes are essentially equal. Typical dependences of carrier lifetime upon injection level, measured by TRPL, is shown in Fig. 10(a) and (b) for 160 μm and 52 μm thick n⁻ epilayers, respectively. A strong dependence on injection is observed between the low-injection and high-injection regimes. Measurements carried out by TFCA at the same position on the 160 μm thick wafer reflect about a factor of 2 longer lifetimes at high injection than the TRPL result, in agreement with theoretical comparisons between the two measurement techniques [62].

The effect on the carrier lifetime of external conditions, such as injection level and temperature, is approached ex-

Figure 10 Injection dependence of the PL decay time for (a) sample A and (b) sample B. The PL decay time is compared in (a) to that determined by TFCA at the same location on the sample. The solid lines are the results of fits of the data to carrier dynamics simulations. Reprinted with permission from Ref. [62], © 2008, American Institute of Physics.

perimentally and from a theoretical point of view, where we assume that the lifetime is determined by SRH recombination at the $Z_{1/2}$ defect, so that Auger and surface recombination are considered negligible. The experiments were arranged to approximate these conditions: Surface recombination is minimized by limiting the measurements to relatively thick layers, as in Fig. 10, and injection levels are limited to $<10^{18}$ cm⁻³, where Auger recombination is negligible [40].

The capture and emission of carriers at defect sites is usually described theoretically by the SRH recombination model [50, 51]. However, this picture assumes a simple defect structure (e.g. two possible charge states – filled and empty) and steady state excitation conditions, and is not directly applicable to a complex defect such as $Z_{1/2}$ and transient excitation. Although much work has been done over the years to extend the SRH model to multi-level systems and to transient conditions [63–69], the problem is not soluble in closed form. Consequently, much of this work has been limited to very high or very low injection, where the problem has relatively simple solutions. This is not a useful approach in the present case, where the variation in the lifetime for arbitrary injection level and temperature is of interest, and where the defect has a more complicated internal level structure. Consequently, we will take the approach of employing numerical carrier dynamics simulations to explore the effects of injection level and temperature on the carrier lifetime and to compare the calculated results to experimental measurements.

The model employed for the simulation is based on the fact (see e.g., Section 2) that $Z_{1/2}$ has been shown to be a –U defect that can trap two electrons, leading to three possible charge states; doubly occupied ("–"), singly occupied ("0") and empty ("+"). Because of the large lattice relaxation around the doubly-occupied Z^- state (see e.g. inset in Fig. 2), the additional repulsive energy associated with the two-electron state is more than offset by the reduction in lattice energy. Consequently, the second electron to be captured is bound more tightly than the first, and the two-electron Z^- state is the equilibrium charge state in n-type material [3]. Transitions between Z^- and Z^0 (–/0), or between Z^0 and Z^+ (0/+), occur through the capture and emission of electrons and holes, and thus affect the carrier lifetime directly. These charge-state transitions are shown schematically in Fig. 11. The energies E_1 and E_2 in the figure represent thermal activation energies for the (–/0) and (0/+) transitions, respectively. As a result of the large lattice relaxation, the (–/0) thermal emission barrier also includes a capture barrier, E_b, as shown in the inset of Fig. 2. The R_{nj} and R_{pj} ($j = 1, 2$) in the figure represent net electron and hole capture rates for the two transitions 1 and 2, corresponding to (–/0) and (0/+), respectively. Solid lines in the figure represent carrier capture, while dotted lines represent the thermal emission of carriers. By employing this model to represent the $Z_{1/2}$ defect in carrier dynamics simulations, the dependence of the carrier lifetime for arbitrary variations in injection level and temperature can be investigated and compared to experiment.
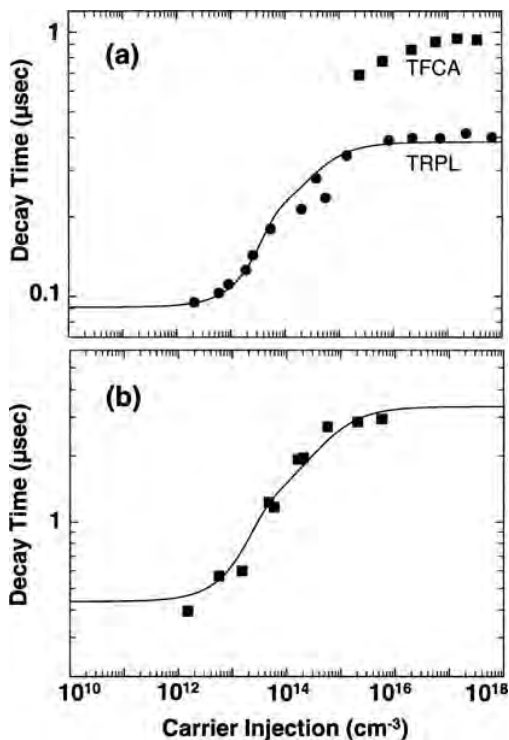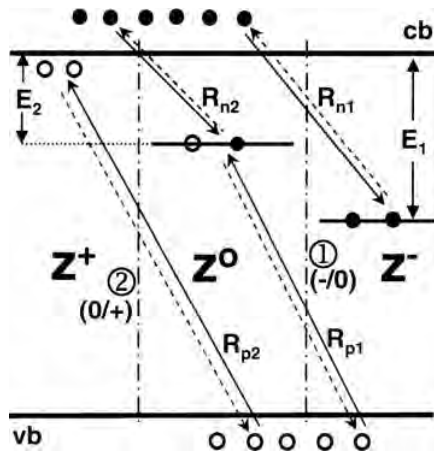
Figure 11 Schematic level scheme for carrier capture and emission at the $Z_{1/2}$ defect. The three charge states of $Z_{1/2}$ (–, 0, +) are indicated, resulting in two transitions: 1 for (–/0) and 2 for (0/+). Transitions due to carrier capture or emission are indicated by solid or dashed arrows, respectively, with corresponding trap depths E_1 and E_2. The net carrier capture rate for each transition is indicated by the R_{nj} and R_{pj}. Reprinted with permission from Ref. [62], © 2008, American Institute of Physics.

4.2 Calculation parameters For the simulation to reflect the experimental situation with reasonable accuracy, the model employed must be a good approximation to the experimental conditions, and an accurate set of material parameters must be available. There is ample evidence that $Z_{1/2}$ dominates the carrier lifetime, as long as the defect concentration is at a non-negligible level [61]. Consequently, SRH recombination at this defect appears to be a reasonable picture, as long as Auger and surface recombination can be neglected. The extent to which the calculated results agree with experimental measurements is sensitive to the particular set of material parameters employed in the calculation. There are some general trends, however, that are noteworthy: The variation of the lifetime with injection level tends to be most sensitive to carrier capture cross-sections and to defect concentrations, while the temperature dependence is most strongly affected by the thermal ionization energies E_1 and E_2, as these enter exponentially in determining the emission rates of the carriers from the deep centers.

Many of the parameters required in the simulations have been measured and are available in the literature. Effective masses for 4H-SiC have been determined by Son et al. [70], while trap depths and electron capture cross-sections for $Z_{1/2}$ were reported by Hemmingsson et al. [3]. Since the material parameters for Z_1 and Z_2 are similar, $Z_{1/2}$ is treated here as a single defect, with averages of the similar parameters for Z_1 and Z_2 reported in Ref. [3] used in the calculation. While Hemmingsson et al. have measured the temperature dependent (0/–) electron capture cross section σ_{n1}, the (+/0) electron capture cross section σ_{n2} reported by this group and by several others falls into a wide range:

Table 2 Parameters used in numerical solution of Eqs. (5)−(7).

parameter	symb	value	Ref.
–/0 trap depth[a]	E_1	0.62 eV	[3]
0/+ trap depth[a]	E_2	0.47 eV	[3]
0/– capture barrier[a]	E_b	0.07 eV	[3]
0/– e⁻ capt.cross section[a]	σ_{n1}	$1.5 \times 10^{-15}\ e^{-0.07/kT}$ cm²	[3]
+/0 e⁻ capt. cross section	σ_{n2}	$\approx (2\text{–}4) \times 10^{-15}$ cm²	c
–/0 h⁺ capt. cross section	σ_{p1}	3.5×10^{-14} cm²	[2]
0/+ h⁺ capt. cross section	σ_{p2}	$\approx (1\text{–}2) \times 10^{-14}$ cm²	c
Z_1/Z_2 concentration[b]	N	$10^{11}\text{–}10^{14}$ cm⁻³	
equilibrium carrier conc.[b]	n_0	$10^{14}\text{–}10^{15}$ cm⁻³	

[a] Average of Z_1 and Z_2 values determined in Ref. [3].
[b] Typical range of concentrations found in n⁻ epilayers.
c Fitted value from simulations.

$\sigma_{n2} \approx (1\text{–}20) \times 10^{-15}$ cm². This uncertainty results from the fact that these values were obtained as an extrapolation of measured data, and whether or not a temperature dependence had been assumed for the capture cross section. Because of this uncertainty, the value of σ_{n2} is estimated here by varying σ_{n2} to fit the experiment. The (–/0) hole capture cross section σ_{p1} has recently been measured [2], but no measurement is available for the (0/+) hole capture cross section, σ_{p2}. Consequently, this parameter is also treated as a variable to be fitted to the experimental results. The other significant parameters in the calculation are the defect concentration N and the equilibrium carrier concentration n_0, which are sample-dependent. In determining σ_{n2} and σ_{p2}, measured values are used for n_0. However, since DLTS measurements were not available for these samples, the defect concentrations are determined from the measured low-injection minority carrier lifetime: $\tau_{MCL} = (a_{p1}N)^{-1}$. Some of the important parameters employed in the simulations are summarized in Table 2. With reasonable fitted values for these two capture cross-sections, generalized simulations can be carried out over a large range of injection level or temperature.

4.3 Experimental TRPL measurements were described in Section 3.2. A flow-through optical cryostat or a temperature-regulated heat stage was used for temperature-dependent measurements. Transient free carrier absorption measurements employed the Nd:YAG laser (Section 3.2) as a pump source, a CW, 1310 nm diode laser (0−5 mW) probe beam and a 0.3 mm diameter InGaAs detector matched to a transimpedance amplifier. Three n⁻ epilayers ($n_0 \approx$ mid 10^{14} cm⁻³ – low-10^{15} cm⁻³) were investigated: Samples A (3″-wafer, 160 μm thick) and B (≈ 1 cm², 52 μm thick) were used for injection dependence studies, and sample C (≈ 1 cm², 160 μm thick) for temperature dependence measurements [62].

4.4 Carrier dynamics simulation Referring to Fig. 11, the SRH carrier lifetime is determined by the capture and emission of electrons and holes. In general, if n and p are electron and hole concentrations defined by

$n(t) = n_0 + \delta n(t)$; $p(t) = p_0 + \delta p(t)$, where the "0" subscripts refer to equilibrium values and δn, δp represent their variations from equilibrium, and with $p_0 \approx 0$ in n-type material, instantaneous carrier lifetimes can be defined as $\tau_n(t) = [-(\mathrm{d}\delta n/\mathrm{d}t)/\delta n)]^{-1}$, $\tau_p(t) = [-(\mathrm{d}\delta p/\mathrm{d}t)/\delta p]^{-1}$. Since the time-varying PL intensity is then of the form $I_{PL}(t) = \gamma[n_0 + \delta n(t)]\,\delta p(t)$, the decay time measured by TRPL can be written $\tau_{PL}(t) = [-(\mathrm{d}I_{PL}(t)/\mathrm{d}t)/I_{PL}(t)]^{-1}$. In terms of the instantaneous electron and hole lifetimes, this can be shown to take the form

$$\frac{1}{\tau_{PL}(t)} = \frac{1}{\tau_p(t)} + \frac{1}{\tau_n(t)}\left[\frac{\delta n(t)}{n_0 + \delta n(t)}\right]. \tag{4}$$

At very low injection ($\delta n \to 0$), the PL decay time is identical with the hole, or minority carrier lifetime, τ_{MCL}, while at very high injection ($\delta n \gg n_0$ and $\tau_n \approx \tau_p = \tau_{HL}$), $\tau_{PL} \to \tau_{HL}/2$ due to the bimolecular recombination kinetics at high injection [62]. Similarly, the time-varying concentrations of the three $Z_{1/2}$ charge states, $Z^k(t)$, $k = (+, 0, -,)$ can be written as $Z^k(t) = Z_0^k + \delta Z^k(t)$. The $\delta Z^k(t)$, $\delta n(t)$ and $\delta p(t)$ constitute the five time-dependent variables defining the problem, of which two can be eliminated, since the total defect concentration N is fixed and charge is conserved:

$$\sum_k \delta Z^k = 0, \qquad \delta n - \delta p = \delta Z^0 + 2\delta Z^+. \tag{5}$$

Eliminating two of the defect concentrations, the time dependence of the carrier and defect concentrations are then determined by

$$\frac{\mathrm{d}\delta n}{\mathrm{d}t} = -(R_{n1} + R_{n2}),$$
$$\frac{\mathrm{d}\delta p}{\mathrm{d}t} = -(R_{p1} + R_{p2}), \tag{6}$$
$$\frac{\mathrm{d}\delta Z^-}{\mathrm{d}t} = R_{n1} - R_{p1},$$

where each of the net capture rates (e.g. Fig. 11) are determined from the difference between capture and emission for each transition, and take the form [62]:

$$R_{n1} = a_{n1}\{(n_0 + \delta n)\,[\delta p - \delta n - 2\delta Z^- + Z_0^0]$$
$$\qquad - n_1[Z_0^- + \delta Z^-]\},$$
$$R_{n2} = a_{n2}\{(n_0 + \delta n)\,[\delta n - \delta p + \delta Z^- + Z_0^+]$$
$$\qquad - n_2[\delta p - \delta n - 2\delta Z^- + Z_0^0]\},$$
$$R_{p1} = a_{p1}[(p_0 + \delta p)\,(Z_0^- + \delta Z^-)] \tag{7}$$
$$\qquad - p_1(\delta p - \delta n - 2\delta Z^- + Z_0^0),$$
$$R_{p2} = a_{p2}[(p_0 + \delta p)\,(\delta p - \delta n - 2\delta Z^- + Z_0^0)$$
$$\qquad - p_2(\delta n - \delta p + \delta Z^- + Z_0^+)].$$

Here, the a_{nj} and a_{pj} are electron and hole capture coefficients; e.g. $a_{nj} = \sigma_{nj}v_{th,n}$, with electron capture cross section σ_{nj} and and hole capture cross section σ_{pj}, respectively,

and $v_{th\,n,p} = (3\,kT/m^*_{e,h})^{1/2}$ are the average carrier thermal velocities. The quantities n_j and p_j are given by [50] $n_j = N_c \exp[-E_j/kT]$ and $p_j = N_v \exp[-(E_g - E_j)/kT]$, with $N_c(T)$ and $N_v(T)$ the effective density of states for the conduction and valence bands, respectively and the E_j denote the energy separations from the conduction band of the two defect levels (–/0) and (0/+).

The primary independent variables of interest are the injection level and the temperature. For a short excitation pulse, the injection level g enters the calculation as an initial condition for the nonequilibrium carrier concentrations: $\delta n(0) = \delta p(0) \equiv g$. The temperature variations of the nonequilibrium carrier concentrations and their lifetimes are determined by the temperature dependent parameters in the calculation: The n_j and p_j vary as $T^{3/2}\exp[-E_j/kT]$ and dominate over the temperature dependence of the a_{nj} and a_{pj}, which vary as $T^{1/2}$, in addition to any temperature variation of the capture cross sections. For $T > 100$ K, the equilibrium carrier concentration is in the saturation range [71], so the equilibrium carrier concentration n_0 may be taken as temperature-independent.

4.5 Simulation results The carrier dynamics simulations provide the time dependence of the nonequilibrium carrier concentrations and the three defect charge state concentrations after a short, above-gap optical pulse, and for varying injection level and temperature. In order to probe the general features of carrier recombination at $Z_{1/2}$, it is first necessary to fit experimental results to Eqs. (4)–(7) in order to obtain consistent values for the two capture cross-sections σ_{n2} and σ_{p2}, so that a full set of parameters (Table 2) is available. The resulting fit of the dependence of TRPL decay time on injection level is shown for samples A and B as the solid lines in Fig. 10(a) and (b). The fitted values for the two capture cross sections for both of these measurements, as well as for the fit of the temperature dependence of the TRPL decay time for sample C, discussed later in this section, all fell within the range $\sigma_{n2} \approx (2-4) \times 10^{-15}$ cm^2 and $\sigma_{p2} \approx (1-2) \times 10^{-14}$ cm^2. With a consistent set of parameters, the general features of carrier dynamics after pulsed excitation can be considered. While the results are dependent on the material parameters employed, e.g. defect concentration and doping level, there are several qualitative features apparent in Table 2 that will have a dominating effect on the results. First, the capture cross section σ_{n1} is much smaller ($\approx 10^{-16}$ cm^2 at room temperature) than the other three cross-sections, so that (–/0) electron capture or emission will be slower, and can be a rate-limiting process. Also, the large depth of the defect levels constrains electron emission to be negligible ($n_1, n_2 \ll \delta n, \delta p$) for $T < 500$ K. Finally, the large band gap of 4H-SiC results in very high barriers (≥ 2.5 eV) for hole emission from these traps. Consequently, hole emission is insignificant ($p_1, p_2 \approx 0$) for temperatures < 1300 K.
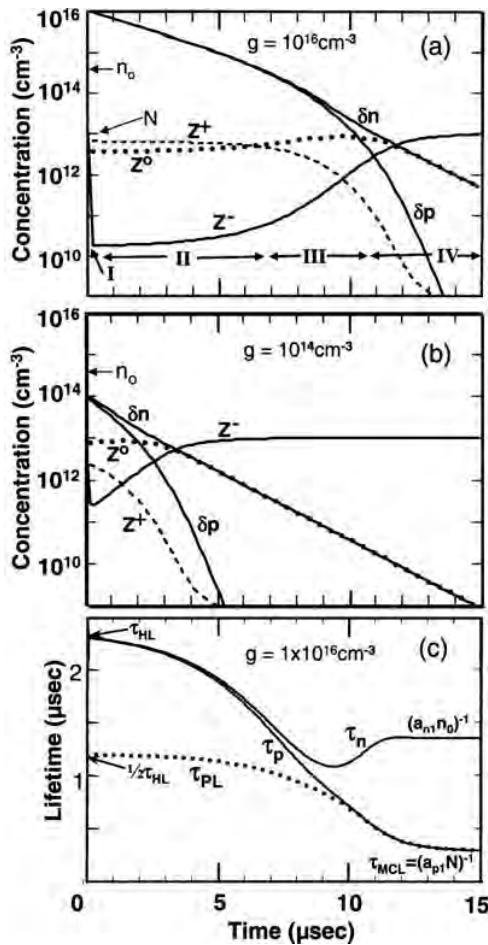
Using the parameters in Table 2, general trends in the carrier dynamics can now be examined. Initially, at room temperature the defects are essentially all in the Z^- state.

Figure 12(a) shows the calculated time dependence, after a short excitation pulse, of the nonequilibrium carrier concentrations, $\delta n(t)$ and $\delta p(t)$, and the three defect charge state concentrations $Z^k(t)$, under high injection conditions, $g = 1 \times 10^{16}$ cm^{-3}, and with typical defect concentration $N = 1 \times 10^{13}$ cm^{-3} and equilibrium carrier concentration $n_0 = 4 \times 10^{14}$ cm^{-3}. The results suggest that the return of the system back to equilibrium follows four main stages of decay, which are indicated by the Roman numerals in the figure. Stage I involves rapid initial hole capture by the equilibrium Z^- state, on a time scale $(a_{p1}g)^{-1} \approx 240$ ps, which rapidly depletes the Z^- concentration and builds up the Z^0 and Z^+ populations.

Stage II is a "high-injection stage", where δn, $\delta p \gg n_0$, N, and therefore $\delta n \approx \delta p$, so that the electron and hole

Figure 12 Simulated time dependence of the carrier concentrations and defect charge states following a short, above-gap optical pulse, for (a) 1×10^{16} cm^{-3} initial injection and (b) 1×10^{14} cm^{-3} initial injection. In (a) four stages of decay of the carrier system are indicated, as discussed in the text. The corresponding evolution of the PL and carrier lifetimes are shown in (c). Reprinted with permission from Ref. [62], © 2008, American Institute of Physics.

lifetimes are approximately equal: $\tau_n \approx \tau_p = \tau_{HL}$. This phase of the carrier recombination can be understood by first considering the behavior of the charge state populations for the case where $T < 500$ K, so that thermal emission is negligible (although the result is easily extended to higher temperature [62]). The time dependence of the Z^- and Z^+ concentrations are then determined by: $dZ^-/dt = R_{n1} - R_{p1}$ and $dZ^+/dt = R_{p2} - R_{n2}$, which can be written, using Eq. (7) in the limit of high injection, as:

$$\frac{dZ^-}{dt} + a_{p1}\delta n Z^-(t) = a_{n1}\delta n Z^0(t) \,,$$

$$\frac{dZ^+}{dt} + a_{n2}\delta n Z^+ = a_{p2}\delta n Z^0 \,. \tag{8}$$

The characteristic times over which Z^- and Z^+ (and thus Z^0) vary, $(a_{p1}\delta n)^{-1}$ and $(a_{n2}\delta n)^{-1}$, respectively, are short at high injection: 240 ps and 1.5 ns, respectively, at 1×10^{16} cm^{-3} injection. For much longer times, the $Z^k(t)$ approach their constant, quasi-steady-state (QSS) values ($t \to \infty$, $dZ^k/dt \to 0$). Therefore, the $Z^k(t)$ concentrations remain slow-varying at their QSS levels as long as the decaying carrier concentration is still in the high-injection regime. This can be seen in the slow-varying charge state concentrations in Fig. 12(a) within Stage II. Under QSS conditions, Eq. (8) becomes an algebraic equation, which can be solved (with $\Sigma Z^k = N$) for the individual QSS charge state concentrations in terms of N and the capture coefficients.

As the decaying carrier concentration approaches n_0, the high injection limit no longer applies, the electron and hole lifetimes begin to diverge and the decay enters into Stage III, a transition between high and low injection. Here the depleted Z^- population begins to increase via 0/– electron capture, while Z^+ decreases via +/0 electron capture. The increasing Z^- concentration leads to an acceleration of –/0 hole capture, resulting in a rapid decrease in the hole lifetime. Stage III is essentially identical to the decay at low initial injection, $g = 1 \times 10^{14}$ cm^{-3}, shown in Fig. 10(b), except for a rigid time shift of several microseconds, which roughly corresponds to the duration of Stage II under high injection.

The last stage of decay, Stage IV, is characterized by low-injection. Here, $\delta p \ll \delta n \ll n_0$ and $Z^- \approx N$. The concentration of the few remaining nonequilibrium electrons is identical to the concentration of Z^0, and decays in the low-injection limit with lifetime $\tau_n \to (a_{n1}n_0)^{-1}$, while the hole lifetime is the minority carrier lifetime, $\tau_p \to (a_{p1}N)^{-1}$.

The carrier dynamics in Fig. 12(a) can also be described by the time dependence of the instantaneous carrier lifetimes, as shown in Fig. 12(c). Here, Stage II ($\tau_n \approx \tau_p$) and Stage IV (τ_n, $\tau_p \approx$ constant) are quite apparent. The PL decay time is also shown, with high-injection behavior ($\tau_{PL} \approx \tau_{HL}/2$) at early times and low-injection behavior ($\tau_{PL} \approx \tau_p$) at later times, after the nonequilibrium carrier concentration has decayed substantially.

Phys. Status Solidi A **206**, No. 10 (2009)

2269

Feature
Article

From Fig. 11 it is clear that we can write $d\delta n/dt = -[a_{n1}nZ^0 + a_{n2}nZ^+]$. Under high injection conditions, where $Z^k \approx Z^k_{QSS}$ and $n \approx \delta n$, the carrier lifetime can be written as $\tau_n^{-1} = \tau_{HL}^{-1} = -[(d\delta n/dt)/\delta n] = -[a_{n1}Z^0_{QSS} + a_{n2}Z^+_{QSS}]$, where the Z^k_{QSS} are determined in terms of N and the capture coefficients, as noted above. Consequently, with $\tau_{MCL} = (a_{p1}N)^{-1}$, the ratio of the high and low injection lifetimes, (τ_{HL}/τ_{MCL}) can be determined in terms of the capture coefficients [62]:

$$(\tau_{HL}/\tau_{MCL}) = \frac{a_{p1}\left(1+\dfrac{a_{p2}}{a_{n2}}+\dfrac{a_{n1}}{a_{p1}}\right)}{a_{n1}+a_{p2}}. \qquad (9)$$

For $a_{n1} \ll a_{n2}, a_{p1}, a_{p2}$, appropriate for $Z_{1/2}$, this simplifies to $\tau_{HL}/\tau_{MCL} \approx a_{p1}(a_{n2}+a_{p2})/a_{n2}a_{p2}$. Using the parameters in Table 2, we find $(\tau_{HL}/\tau_{MCL}) \approx 10$. Incorporating the additional factor of 1/2 for the high-injection PL lifetime ($\tau_{PL} \approx \tau_{HL}/2$), the same ratio for PL decay times becomes $(\tau_{HL}/\tau_{MCL})_{PL} \approx 5$, which agrees quite well with the measured high- and low-injection PL lifetimes in Fig. 10.

Simulations were also carried out assuming that *both* traps, $Z_{1/2}$ and $EH_{6/7}$, contribute significantly to the recombination. While the electron capture cross section for $EH_{6/7}$ has been measured as $\sigma_{n3} = 5 \times 10^{-15}$ cm^2 at room temperature [72], there is no measurement available for the hole capture cross section, σ_{p3}. Since DLTS measurements in forward biased p–i–n diodes indicate this parameter to be small [2, 58], a value of 1×10^{-17} cm^2 was adopted for the simulations. The results, similar to Fig. 12(a), indicated little effect on the carrier lifetimes until the $EH_{6/7}$ concentration was increased far beyond what is observed in as-grown material. It is apparent that the small hole capture cross-section for this defect limits its role as an effective recombination center, although the large electron capture cross section and large thermal ionization energy (≈ 1.6 eV) make it an effective trapping center for majority carriers.

The change in the carrier lifetime with varying temperature was also considered, both experimentally and through carrier dynamics simulations. The calculated carrier lifetime is affected by temperature in two ways; through the temperature dependence of the capture and emission rates and through the temperature dependence of the equilibrium distribution of the three $Z_{1/2}$ charge states. The latter is taken into account in the simulation as a temperature dependent initial condition in the solution of Eq. (6). It was noted earlier that the temperature dependence of the carrier lifetime controlled by SRH recombination at the $Z_{1/2}$ defect will be dominated by the exponential dependence associated with thermal emission from deep traps, and that hole emission will be negligible except at the highest temperatures. Consequently, electron emission is expected to dominate the temperature dependent lifetime. Since the thermal emission of trapped carriers tends to repopulate the decaying free carrier concentration, enhanced carrier emission due to increased temperature is expected to lead to a corresponding increase in the carrier lifetime.

This increase is also observed experimentally [38, 62]. In Fig. 13(a), the temperature dependence of the PL decay time, measured for sample C (open squares), is compared to the results of the simulation (filled circles). The calculation reproduces the observed rapid increase in lifetime above 500 K reasonably well. The resulting fitting parameters were $\sigma_{n2} = 3 \times 10^{-15}$ cm^2 and $\sigma_{p2} = 1.4 \times 10^{-14}$ cm^2, which are consistent with the corresponding parameters determined previously by fitting the injection dependences of the lifetime for samples A and B. The experimental points are compared in the figure to data reported by Kordina et al. [38], and agree reasonably well over their common range of temperatures. However, the measurements do not reflect the sharpness of the "knee" in the simulation near 500 K. This may well result from limitations in the model of Fig. 11, which assumes contribution from only a single defect. The more gradual rise in the lifetime with temperature below 500 K is consistent with a small contribution to the lifetime from other defects with lower thermal activation energies than $Z_{1/2}$, such as the boron hole trap ($E_v + 0.27$ eV), which is filled in n-type material and available to trap nonequilibrium minority holes.
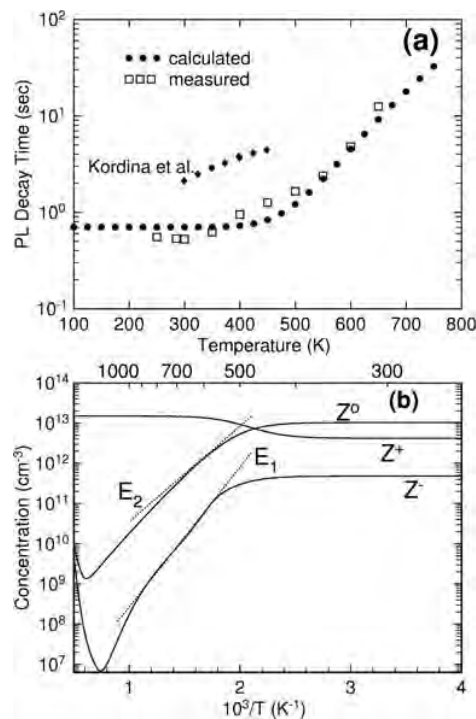
Figure 13 (a) Measured temperature dependence of the PL lifetime for sample C (open squares) compared to the simulated behavior (solid circles). Measurements reported in Ref. [38] are shown as filled diamonds. (b) The simulated temperature dependence of the three Z_1/Z_2 charge state concentrations for $t \approx 0.5$ µs. Reprinted with permission from Ref. [62], © 2008, American Institute of Physics.

The dominant temperature dependence responsible for the rapid rise in lifetime above 500 K was found to result from electron emission from Z^0, which is expected, as this transition involves the smallest of the two activation energies. The nature of the transition can be seen clearly from the simulation: The simulated temperature dependence of each of the three $Z_{1/2}$ charge states is shown in Fig. 13(b), for $t = 0.5\ \mu s$ after the exciting pulse. It is apparent from the figure that as temperature increases toward 500 K, the Z^+ concentration begins to increase, while the Z^0 concentration decreases exponentially, with an activation energy near that of E_2. These are the hallmarks of a 0/+ transition resulting from the thermal emission of electrons from Z^0. The much smaller Z^- concentration also decreases, with thermal activation energy E_1, reflecting –/0 electron emission. As temperature is increased further, Z^0 and Z^- concentrations continue to decline until, at very high temperatures, hole emission $Z^0 \rightarrow Z^-$ (>1300 K) and $Z^+ \rightarrow Z^0$ (>1600 K) become significant, and these two charge states begin to increase in population with increasing temperature.

5 Summary In the preceding, we have followed the progress toward understanding the identity, the local structure and the recombination dynamics of the defects that control the carrier lifetime in n-type 4H-SiC epitaxial layers. Over the course of about a decade, the results of many measurements concluded that two defects, $Z_{1/2}$ and $EH_{6/7}$, both dominant electron traps in DLTS spectra, were responsible for controlling the carrier lifetime. Over about the same time period, a progression of DLTS studies were carried out with varying growth temperature, C/Si ratio, thermal anneal temperature, electron irradiation and ion implantation, concluding that the structure of both of these defects involved a carbon vacancy.

However, later studies showed that the observed correlations between the carrier lifetime and *both* $Z_{1/2}$ and $EH_{6/7}$ could result from the fact that the two defects, sharing a similar structure, tend to vary in concentration in a similar manner in response to changes in growth or post-growth processing parameters. Thus, the same correlation of both defects with the lifetime would be observed, even if only one of the two defects had a significant impact on the carrier lifetime. This possibility was confirmed experimentally: Individual cases were observed where only $Z_{1/2}$ was correlated to the carrier lifetime, and DLTS studies of forward biased p–i–n diode structures indicated that $EH_{6/7}$ has a small cross capture section for minority holes, and cannot be the dominant minority carrier trap. Consequently, it was concluded that $Z_{1/2}$ alone is the lifetime killer in this material.

This has led to some interest in the details of the recombination processes occurring at the $Z_{1/2}$ center. To this end, transient carrier decay measurements have been carried out over a wide range of carrier injection levels and temperatures, and were compared to the behavior calculated for this complex defect. Since the carrier dynamics problem has no closed form solution for arbitrary injection

level and temperature, simulations were performed using material parameters available in the literature. Two capture cross-sections that have not been determined uniquely were employed as fitting parameters, and the resulting values were found consistent for three independent sets of lifetime measurements. Using a consistent set of parameters, the generalized simulations provided insight into the details of carrier recombination at $Z_{1/2}$. The response of the system to a short, above-gap optical pulse was observed to follow four distinct stages of decay for the nonequilibrium electron and hole concentrations and the populations of the three $Z_{1/2}$ charge states. A high-injection phase, following the rapid capture of minority holes by the equilibrium Z^- state, was characterized by slow-varying, quasi-steady-state defect charge state concentrations, as both carrier types decayed at the high-injection limit, τ_{HL}. A transition to the low-injection regime followed, as the decaying non-equilibrium carrier concentration approached the doping level. The temperature dependence of the carrier lifetime was found to be relatively weak below 500 K, but increased rapidly above this temperature, as electrons trapped in the Z^0 charge state are thermally emitted into the conduction band. At higher temperatures, contributions due to electron emission from the deeper Z^- state occur. Due to the very large emission barrier, hole emission does not become significant until very high temperature (≥ 1300 °C).

References

[1] K. Danno, D. Nakamura, and T. Kimoto, Appl. Phys. Lett. **90**, 202109 (2007).
[2] P. B. Klein, B. V. Shanabrook, S. W. Huh, A. Y. Polyakov, M. Skowronski, J. J. Sumakeris, and M. J. O'Loughlin, Appl. Phys. Lett. **88**, 052110 (2006).
[3] C. G. Hemmingsson, N. T. Son, A. Ellison, J. Hang, and E. Janzén, Phys. Rev. B **58**, R10119 (1998).
[4] W. Suttrop, G. Pensl, and P. Lanig, Appl. Phys. A **51**, 231 (1990).
[5] M. S. Mazzola, S. E. Saddow, P. G. Neudeck, V. K. Lakdawala, and S. We, Appl. Phys. Lett. **64**, 2730 (1994).
[6] A. Uddin, H. Misuhashi, and T. Uemoto, Jpn. J. Appl. Phys. **33**, L908 (1994).
[7] T. Kimoto, A. Itoh, H. Matsunami, S. Sridhara, L. L. Clemen, R. P. Devaty, W. J. Choyke, T. Dalibor, C. Peppermüller, and G. Pensl, Appl. Phys. Lett. **67**, 2833 (1995).
[8] G. Pensl and W. J. Choyke, Physica B **185**, 264 (1993).
[9] H. Zhang, Ph.D. thesis, Erlangen (1990).
[10] H. Zhang, G. Pensl, A. Dörnen, and S. Leibenzeder, Ext. Abstr. Electrochem. Soc. **89**(2), 699 (1989).

Phys. Status Solidi A 206, No. 10 (2009)

2271

[11] J. P. Doyle, M. O. Aboelfotoh, M. K. Linnarsson, B. G. Svensson, A. Schöner, N. Nordell, C. Harris, J. L. Lindström, E. Janzén, and C. Hemmingsson, MRS Symp. Proc. Ser. **423**, 519 (1996).

[12] T. Dalibor, C. Peppermüller, G. Pensl, S. Sridhara, R. P. Devaty, W. J. Choyke, A. Itoh, T. Kimoto, and H. Matsunami, Inst. Phys. Conf. Ser. **142**, 517 (1996).

[13] T. Dalibor, G. Pensl, T. Kimoto, H. Matsunami, S. Sridhara, R. P. Devaty, and W. J. Choyke, Diam. Relat. Mater. **6**, 1333 (1997).

[14] L. Patrick and J. W. Choyke, Phys. Rev. B **5**, 3253 (1972).

[15] L. Storasta, F. H. C. Carlsson, S. G. Sridhara, J. P. Bergman, A. Henry, T. Egilsson, A. Hallén, and E. Janzén, Appl. Phys. Lett. **78**, 46 (2001).

[16] C. G. Hemmingsson, N. T. Son, O. Kordina, J. P. Bergman, E. Janzén, J. L. Lindström, S. Savage, and N. Nordell, J. Appl. Phys. **81**, 6155 (1997).

[17] C. G. Hemmingsson, N. T. Son, A. Ellison, J. Hang, and E. Janzén, Phys. Rev. B **59**, 7768 (1999).

[18] T. Kimoto, S. Nakazawa, K. Hashimoto, and H. Matsunami, Appl. Phys. Lett. **79**, 2761 (2001).

[19] A. Kawasuso, F. Redmann, R. Krause-Rehberg, M. Weidner, T. Frank, G. Pensl, P. Sperr, W. Triftshäuser, and H. Itoh, Appl. Phys. Lett. **79**, 3950 (2001).

[20] I. Pintilie, L. Pintilie, K. Imscher, and B. Thomas, Appl. Phys. Lett. **81**, 3950 (2002).

[21] T. A. G. Eberlein, R. Jones, and P. B. Briddon, Phys. Rev. Lett. **90**, 225502 (2003).

[22] L. Storasta, A. Henry, J. P. Bergman, and E. Janzén, Mater. Sci. Forum **457–460**, 469 (2004).

[23] L. Storasta, J. P. Bergman, A. Henry, E. Janzén, and J. Lu, J. Appl. Phys. **96**, 4909 (2004).

[24] A. Castaldini, A. Cavallini, and I. Rigutti, Semicond. Sci. Technol. **21**, 724 (2006).

[25] J. Zhang, L. Storasta, J. P. Bergman, N. T. Son, and E. Janzén, J. Appl. Phys. **93**, 4708 (2003).

[26] T. Kimoto, K. Hashimoto, and H. Matsunami, Jpn. J. Appl. Phys. **42**, 7294 (2003).

[27] H. Fujiwara, K. Danno, T. Kimoto, T. Tojo, and H. Matsunami, J. Cryst. Growth **281**, 370 (2005).

[28] K. Danno, T. Hori, and T. Kimoto, J. Appl. Phys. **101**, 053709 (2007).

[29] Y. Negoro, T. Kimoto, and H. Matsunami, Appl. Phys. Lett. **85**, 1716 (2004).

[30] G. Alfieri, E. V. Monakhov, B. G. Svensson, and M. K. Linnarsson, J. Appl. Phys. **98**, 043518 (2005).

[31] K. Danno, T. Kimoto, and H. Matsunami, Appl. Phys. Lett. **86**, 122104 (2005).

[32] C. W. Litton, D. Johnstone, S. Akarca-Biyikli, K. S. Ramalah, I. Bhat, T. P. Chow, J. K. Kim, and E. F. Schubert, Appl. Phys. Lett. **8**, 121914 (2006).

[33] K. Danno and T. Kimoto, J. Appl. Phys. **100**, 113728 (2006).
   T. Kimoto, K. Danno, and J. Suda, Phys. Status Solidi B **245**, 1327 (2008).

[34] A. Zywietz, J. Furthmüller, and F. Bechstedt, Phys. Rev. B **59**, 15166 (1999).

[35] L. Torpo, M. Marlo, T. E. M. Staab, and R. M. Nieminen, J. Phys.: Condens. Matter **13**, 6203 (2001).

[36] N. T. Son, B. Magnusson, and E. Janzén, Appl. Phys. Lett. **81**, 3945 (2002).

[37] T. A. G. Eberlein, R. Jones, P. R. Briddon, and S. Oberg, Mater. Res. Soc. Proc. **864**, 3 (2005).

[38] O. Kordina, J. P. Bergman, A. Hallén, and E. Janzén, Appl. Phys. Lett. **69**, 679 (1996).

[39] A. Galeckas, V. Grivickas, and J. Linnros, J. Appl. Phys. **81**, 3522 (1997).

[40] V. Grivickas, A. Galeckas, and J. Linnros, Lith. Phys. J. **37**, 473 (1997).

[41] J. P. Bergman, A. Ellison, A. Henry, L. Storasta, and E. Janzén, Semiconducting and Insulating Materials XI (IEEE, Piscataway, N. J., USA, 2000), p. 283.

[42] E. Janzén, A. Henry, J. P. Bergman, A. Ellison, and B. Magnusson, Mater. Sci. Semicond. Process. **4**, 181 (2001).

[43] T. Mori, M. Kato, H. Watanabe, M. Ichimura, E. Arai, S. Sumie, and H. Hashizume, Jpn. J. Appl. Phys. **44**, 8333 (2005).

[44] A. A. Lebedev, D. V. Davydov, N. S. Savkina, A. S. Tregubova, M. P. Shcheglov, R. Yakimova, M. Syväjärvi, and E. Janzén, Semiconductors **34**, 1133 (2000).

[45] H. Iwata, U. Lindefelt, S. Öberg, and P. R. Briddon, Phys. Rev. B **65**, 033203 (2002).

[46] S. I. Maximenko, J. A. Freitas, Jr., P. B. Klein, A. Shrivastava, and T. S. Sudarshan, Appl. Phys. Lett. **94**, 092101 (2009).

[47] L. Storasta, J. P. Bergman, C. Hallin, and E. Janzén, Mater. Sci. Forum **389–393**, 549 (2002).

[48] H. Tsuchida, I. Kamata, S. Izumi, T. Tawara, T. Jikimoto, T. Miyanagi, T. Nakamura, and K. Izumi, Mater. Res. Soc. Proc. **815**, 35 (2004).

[49] J. R. Jenny, D. P. Malta, V. F. Tsvetkov, M. K. Das, H. McD. Hobgood, C. H. Carter, Jr., R. J. Kumar, J. M. Borrego, R. J. Gutmann, and R. Aavikko, J. Appl. Phys. **100**, 113710 (2006).

[50] W. Shockley and W. T. Read, Phys. Rev. **87**, 835 (1952).

[51] R. N. Hall, Phys. Rev. **87**, 387 (1952).

[52] A. B. Sproul, J. Appl. Phys. **76**, 2851 (1994).

[53] P. Grivickas, J. Linnros, and V. Grivickas, J. Mater. Res. **16**, 524 (2000).

[54] P. B. Klein, B. V. Shanabrook, S. W. Huh, A. Y. Polyakov, M. Skowronski, J. J. Sumakeris, M. J. O'Loughlin, Electrochem. Soc. Trans. **3**, 19 (2006).

[55] S. W. Huh, J. J. Sumakeris, A. Y. Polyakov, M. Skowronski, P. B. Klein, B. V. Shanabrook, M. J. O'Loughlin, and A. V. Govorkov, Mater. Sci. Forum, **527–529**, 493 (2006).

[56] K. Fujihira, T. Kimoto, and H. Matsunami, Appl. Phys. Lett. **80**, 1586 (2002).

[57] J. ul Hassan, C. Hallin, J. P. Bergman, and E. Janzén, Mater. Sci. Forum **527–529**, 183 (2006).

[58] S. A. Reshanov, W. Bartsch, B. Zippelius, and G. Pensl, Proceedings ECSCRM 2008, Mater. Sci. Forum (2009), in press.

[59] L. Storasta and H. Tsuchida, Appl. Phys. Lett. **90**, 062116 (2007).

[60] L. Storasta, H. Tsuchida, T. Miyazawa, and T. Ohshima, J. Appl. Phys. **103**, 013705 (2008).

[61] K. Danno, D. Nakamura, and T. Kimoto, Appl. Phys. Lett. **90**, 202109 (2007).

[62] P. B. Klein, J. Appl. Phys. **103**, 033702 (2008).

[63] D. J. Sandiford, Phys. Rev. **105**, 524 (1957).
[64] G. K. Wertheim, Phys. Rev. **109**, 1086 (1958).
[65] K. C. Nomura and J. S. Blakemore, Phys. Rev. **112**, 1607 (1958).
[66] K. C. Nomura and J. S. Blakemore, Phys. Rev. **121**, 734 (1961).
[67] B. G. Streetman, J. Appl. Phys. **37**, 3137 (1966).
[68] C. T. Sah and W. Shockely, Phys. Rev. **109**, 1103 (1958).

[69] S. C. Choo, Phys. Rev. B **1**, 687 (1970).
[70] N. T. Son, P. N. Hai, W. M. Chen, C. Hallin, B. Monemar, and E. Janzén, Phys. Rev. B **61**, R10544 (2000).
[71] S. M. Sze, Physics of Semiconductors, 2nd ed. (John Wiley & Sons, New York, 1981), p. 25.
[72] C. G. Hemmingsson, N. T. Son, O. Kordina, E. Janzén, J. L. Lindström, S. Savage, and N. Nordell, Mater. Sci. Eng. B **46**, 336 (1997).